International Journal of Engineering Trends and Technology
ISSN: 2231–5381 / https://doi.org/10.14445/22315381/IJETT-V71I4P224

Volume 71 Issue 4, 274-283, April 2023

Original Article

Automated Wireless Capsule Endoscopy Image Classification using Reptile Search Optimization with Deep Learning Model

M. Amirthalingam[1], R. Ponnusamy[2]

[1,2]*Department of Computer and Information Science, Annamalai University, Annamalai Nagar, India*

[1]*Corresponding Author : amir.cdm@gmail.com*

Received: 25 February 2023 Revised: 31 March 2023 Accepted: 13 April 2023 Published: 25 April 2023

Abstract *- Wireless Capsule Endoscopy (WCE) is one of the effective ways of investigating Gastrointestinal Tract (GI) diseases and implementing painless intestine imaging. Regardless, numerous concerns make its adaptation and extensive applicability challenges as tolerance, efficiency, performance, and safety. In addition, automatic investigation of the WCE information is more important for abnormality detection. Imaging a patient's gastrointestinal tract through WCE generates large data that necessitates a special skill set from a medical practitioner and a substantial amount of time for analysis. Numerous vision and computer-aided -based solutions were introduced to overcome these challenges, yet, they do not offer the desired level of accuracy and further enhancement is still required. Therefore, this article presents an Automated Wireless Capsule Endoscopy Image Classification using Reptile Search Optimization with Deep Learning (WCEIC-RSADL) algorithm. The presented WCEIC-RSADL approach examines the WCE images using DL and hyperparameter tuning techniques. To achieve this, the presented WCEIC-RSADL technique involves bilateral filtering (BF) technique employed for the noise elimination process. Moreover, the presented WCEIC-RSADL technique enables the Inception v2 model for feature extraction purposes with RSA-based hyperparameter tuning purposes. Furthermore, the extreme learning machine (ELM) method can be exploited for WCE image classification. In order to exhibit the enhanced achievement of the WCEIC-RSADL approach, an extensive range of simulations were executed on the WCE image dataset. The results pointed out that the WCEIC-RSADL algorithm reaches promising performance over other approaches.*

Keywords *- Wireless capsule endoscopy, Deep learning, Image classification, Hyperparameter tuning, Reptile search algorithm.*

1. Introduction

Wireless Capsule Endoscopy (WCE) may be denoted as a non-invasive approach leveraged for identifying irregularities in the GI tract [1]. It looks like a capsule having a length of 26 mm by 11 mm, containing a battery, illuminator, optical dome, RF transmitter, and image sensor [2]. In the evaluation, the patients swallowed WCE and transferred it over the diminutive intestine in a slow manner, and while moving, it considered images of the complete GI tract [3]. Decisively, such images were sent via a wireless technique to a data recording device for physicians to inspect the imageries later for detection. Fifty thousand to sixty thousand images are captured while traveling over the GI tract [4]. The doctor should validate the 60,000 pictures to identify any abnormalities that exist in the GI tract; it reminded a dreary and time-utilizing technique [5]. Therefore, Computer-Aided Detection (CAD) techniques are modelled to overcome the recent practices.

With the large quantity of images, it needs a considerable period for a doctor to scrutinize such images, which may be burdensome for the doctor and result in misdiagnosis of the infected area of the intestine [7]. Accordingly, detecting images with infected regions through several ML and statistical algorithms was an attractive research area in the last decade [8]. An automated detection mechanism executes analysis of the images on a large scale. It identifies the diseased frames, so it will be easier for the doctor to scrutinize only such frames that cover visual contents of the infected area and start suitable remedial action promptly [9]. ML approaches have shown important competence in doing automated tasks and hold the potential to make the medical field more accurate and advanced [10]. Several research scholar work on automated mechanisms for GI tract infection classification and GI infection detection utilizing artificial intelligence (AI) [11]. This study mainly focused on classifying GI tract infection (bleeding) images using the ML pattern.

This article presents an Automated Wireless Capsule Endoscopy Image Classification using Reptile Search Optimization with Deep Learning (WCEIC-RSADL) approach. The presented WCEIC-RSADL technique involves bilateral filtering (BF) technique employed for the noise elimination process. Moreover, the presented WCEIC-RSADL technique enables the Inception v2 model for feature extraction purposes with RSA-based hyperparameter tuning purposes. Furthermore, the extreme learning machine (ELM) model was exploited for WCE image classification. In order to exhibit the enhanced achievement of the WCEIC-RSADL approach, an extensive range of simulations were executed on the WCE image dataset.

2. Related Works

Souaidi and El Ansari [12] presented a hybridized networking of an InceptionV4 structure-related Single-Shot Multibox Detector (Hyb-SSDNet) for finding smaller polyp areas in colonoscopy frames and WCE. Medical privacy concerns remain to be key blockades for acquiring WCE images. The author enlarged the trained data and inspected deep TL methods to fulfil the object recognition necessities. The Hyb-SSDNet structure adopted inception blocks to alleviate inherent limits of the convolution process for incorporating semantic information and contextual features into deep networks. The authors [14] presented the lesion attention-aware CNN method utilizing the self-attention system for the localization of the lesion sections in WCE imageries. The introduced novel lesion area estimating approach leverages ResNet-50 as a self-attention mechanism and convolutional stem that precisely incorporate spatial aspects in a global context for localising the lesion attention mappings in WCE imagery. In [15], a hybrid CNN was devised for abnormality recognition that derives a rich pool of useful attributes from WCE through various convolutional operations. A new meta-feature extracting system was presented in the third network for extracting paradigms from statistical data drawn over features produced from the second and first networks and their preceding layer. In [17], the author formulated CNN for independent recognition of colorectal polyps, and it is an enhanced version of ZF-Net that leverages integration of TL, data augmentation and preprocessing. The author further positioned CNN as a foundation for Faster RCNN for localizing locations of imagery comprising colorectal polyps.

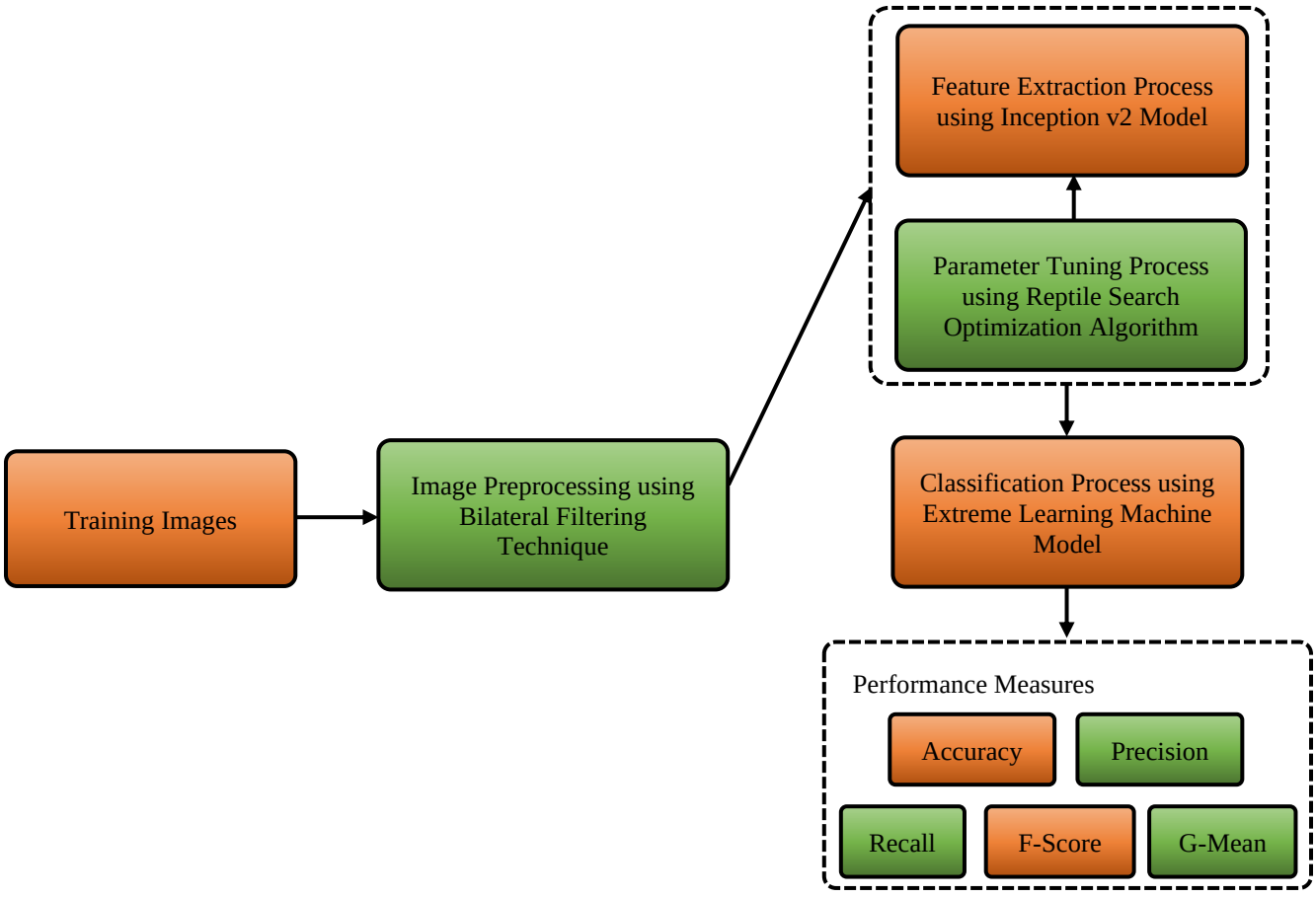

Fig. 1 Workflow of WCEIC-RSADL system

Biniaz et al. [18] introduced a new capsule video summarization structure for minimalizing WCE reviewing hours through factorizing investigation depending on sliding window Singular Value Decomposition (SVD). Adaptive sliding window SVD was employed for extracting the salient video frames. Souaidi and El Ansari [20] examine various structures of pre-trained CNN from scratch for the WCE polyp classifier task. The experimentations reliably prove that using a familiar DCNN structure called Inception V3 with suitable fine parameter tuning outperforms it. The last FC layer was linked to the SVM classifier to gain superior precision.

3. The Proposed Model

We have developed a WCEIC-RSADL method for WCE image categorization in this research. The introduced WCEIC-RSADL approach mainly concentrated on categorising the WCE images using DL and hyperparameter tuning techniques. The WCEIC-RSADL technique comprises BF-based preprocessing, Inception v2-based feature extraction, RSA-based parameter tuning, and ELM-based categorization. Fig. 1 determines the workflow of the WCEIC-RSADL model.

3.1. Image Preprocessing

Primarily, the introduced WCEIC-RSADL approach involves the BF technique employed for the noise elimination process. The BF changes the central pixels of every filter window with the weighted average of its neighboring colour pixel [21]. The weighted function has been intended to smooth the region of relating colors while keeping edges together with heavily weighted individual pixels that are either spatial close or photometrical compared with the central pixel. Demonstrated by $||\cdot||_2$ the Euclidean norms and $\mathrm{F_u}$ the concerning central pixel. Then, the weighted $\mathcal{W}(\mathrm{F_u}, \mathrm{F_v})$ corresponding to any pixels $\mathrm{F_v}$ as provided $\mathrm{F_u}$ states the product of two components, 1 spatial and 1 photometrical

$$\mathcal{W}(\mathrm{F_u}, \mathrm{F_v}) = \mathcal{W}_s(\mathrm{F_u}, \mathrm{F_v})\mathcal{W}_p(\mathrm{F_u}, \mathrm{F_v}) \quad (1)$$

but the spatial component $\mathcal{W}_s$ $(\mathrm{F_u}, \mathrm{F_v})$ can be defined as follows:

$$\mathcal{W}_s(\mathrm{F_u}, \mathrm{F_v}) = e^{-\frac{||\mathrm{u}-\mathrm{v}||_2^2}{2\sigma_S^2}} \quad (2)$$

and the photometrical element $\mathcal{W}_p(\mathrm{F_u}, \mathrm{F_v})$ is defined as follows:

$$\mathcal{W}_p(\mathrm{F_u}, \mathrm{F_v}) = e^{-\frac{\Delta E_{Lab}(\mathrm{F_u}, \mathrm{F_v})^2}{2\sigma_p^2}} \quad (3)$$

where $\Delta E_{Lab} = [(\Delta L^*)^2 + (\Delta a^*)^2 + (\Delta b^*)^2]^{\frac{1}{2}}$ determines perceptual colouring errors from $L^*a^*b^*$ colouring space, and $\sigma_s, \sigma_p > 0$.

3.2. Inception-v2-based Feature Extraction

In this study, the presented WCEIC-RSADL technique derived the Inception v2 model for feature extraction purposes. CNN was one approach of DL. The objective of the training model is to train the ANN to minimalize the error of predictive outcomes with the actual dataset [22]. The input layer was a vector of image datasets. The convolutional layer was a convolutional operation among two vectors. CNN comprises two phases. The initial phase is to group images through the feedforward method. The next phase leverages the BP technique. In this phase, before performing the classifier process, initially perform the cropping and wrapping approaches to concentrate on the object to be categorized. Next, training can be performed by using backpropagation and feedforward approaches. The CNN architecture is separated into two parts, the Fully-Connected and the Feature Extraction Layers. During Feature Extraction, the encoding process takes place, which converts the imagery into factors in the form of numbers. It comprises Pooling and Convolutional Layers. The convolution layer comprises neurons organized to form a filter with height (pixels) and length. A convolutional process is performed between the filter matrices and the input image matrix at this stage. Next, the convolution operation is performed, and the activation function is activated using the ReLU function.

Inception is the expansion of the CNN technique. Inception was initially coined by Szegedy et al. in 2014 in the publication titled "Going Deeper with Convolutions". The inception model for the initial version was InceptionV1. InceptionV1 is used for analyzing the problem to be simpler such that it can be overcome or resolved. InceptionV2 is intended to overcome the deficiencies of InceptionV1. Hence the architecture of InceptionV2 is more efficient than before.

Moreover, the inceptionV3 is much like the V2 inception to overcome the flaws of the prior inception. The InceptionV3 architecture is a progression of GoogLeNet that has featured a 7x7 convolutional layer and is separated into two or three, where layers 3x3 convolutional operation by increasing computation could receive images with 299x299 dimension. InceptionV2 and V3 have four components that are given in the following:

- Change 5x5 to 3x3 convolutional layers.
- Convolution factoring can be performed on the module.
- The module is transformed to be broader so that convolution network complexity can decrease.
- Minimized input size from 35x35 to 17x17.

3.3. Hyperparameter Tuning

The RSA technique is involved in this research for optimum parameter tuning procedure. RSA is a metaheuristic algorithm based on the natural hunting behavior of crocodiles [23]. The working of RSA consists of two stages: encircling and hunting phases. The RSA shift between various stages is executed by dividing the number of iterations into 4 parts and switching between the hunting search and encircling phases. The RSA initiates by the generation of a set of initial solution

candidates as:

$$\chi_{jk} = rand \times (U_b - L_b) + L_b \; k = 1,2, \dots n \quad (4)$$

Where χ_{jk} =initialization matrix, $j = 1,2$ ....P. n signifies dimensions (columns of the initial matrix) of the given optimization problem, and P signifies population size (rows of initial matrix). L_b, U_b, and rand represents the lower boundary, upper boundary, and random number.

During this process, belly and high walking, which depends on crocodile movement, play a crucial role. This movement helps determine a wide search space but does not assist in catching the prey.

$$\chi_{jk(\tau+1)=Best_k(\tau)} \times \left(-\mu_{(jk)}(\tau)\right) \times \beta - \left(R_{(jk)}(\tau) \times rand\right), \tau \leq \frac{T}{4} \quad (5)$$

$$x_{jk}(\tau+1) = Best_k(\tau) \times \chi_{(r_1,k)} \times ES(\tau) \times \; rand, \tau \leq 2\frac{T}{4} \; and \; \tau > \frac{T}{4} \quad (6)$$

Where $Best_k(\tau)$ denotes the best possible solution at k^{th} location, $rand$ characterizes a random integer, τ indicates the existing number of iterations, and the maximal amount of iterations was characterized by T. $\mu_{(j,k)}$ represent the value of hunting operator of j^{th} solution at k^{th} location as:

$$\mu_{(j,k)} = Best_k(\tau) \times P_{(j,k)} \quad (7)$$

Where β indicates a sensitivity parameter, which explains exploration accuracy. Another function called $R_{(j,k)}$, whose aim was to decrease search region, is evaluated by Eq. (8):

$$R_{(j,k)} = \frac{Best_k(\tau) - P_{(r_2,k)}}{Best_k(\tau) + e} \quad (8)$$

Where r_1 indicates the value of the randomly generated number, which ranges from 1 to N. Now, N signifies the overall amount of candidate solutions. $z_{(r1,l)}$ shows the randomly generated location for the k^{th} solution. Also, r_2 denotes a randomly generated value within [1, N], whereas e signifies a value of smaller magnitude. ES (τ), called Evolutionary Sense, was a probability-related ratio and is mathematically formulated by using Eq. (9):

$$ES(\tau) = 2 \times r_3 \times \left(1 - \frac{1}{T}\right) \quad (9)$$

Where r_3 signifies a random number. $P_{(j,k)}$ is evaluated by:

$$P_{(j,k)} = \alpha + \frac{\chi_{(j,k)-M(x_j)}}{Best_k(\tau)x(U_{b(k)} - (L_{b(k)}) + e} \quad (10)$$

In Eq. (10), α denotes the sensitivity limit which controls the exploration accuracy $M(\chi_j)$ indicates the average position of j_{th} solution as:

$$M(\chi_{j)=\frac{1}{n}} \sum_{k=1}^{n} \chi_{(j,k)} \quad (11)$$

The hunting stage, like the encircling stage, has two approaches, such as hunting cooperation and coordination. Also, based on the iteration hunting stage can be divided into 2 portions. The hunting cooperation strategy is held from $\tau \leq T$ and $\tau > 3\frac{T}{4}$, while the hunting coordination was held for iteration ranges from $\tau \leq 3\frac{T}{4}$ and $> 2\frac{T}{4}$. Stochastic coefficient is used to traverse the search space locally to produce the best possible solution. The exploitation stage can be given as follows:

$$x(j,k)(\tau+1) = Best_k(\tau) \times \left(P_{(j,k)}(\tau)\right) \times rand, \tau \leq 3\frac{T}{4} \; and \; \tau > 2\frac{T}{4} \quad (12)$$

$$x(j,k)(\tau+1) = Best_k(\tau) - \mu_{(j,k)}(\tau) \times e - R_{(j,k)}(\tau) \times rand, \tau \leq T \; and \; \tau > 3\frac{T}{4} \quad (13)$$

Where $Best_k(\tau)$ denotes the k^{th} location in the optimum solution at the present iteration. Likewise, $\mu_{(j,k)}$ characterizes the hunting operator that is evaluated using Eq. (7).

The RSA system developed a Fitness Function (FF) for attaining greater categorizer outputs. It determined positive values for demonstrating the best candidate outcomes. In such a case, the minimized classifier error rate was treated that FF was expressed in Eq. (14).

$$fitness(x_i) = ClassifierErrorRate(x_i) = \frac{number\ of\ misclassified\ sampling}{Total\ number\ of\ sampling} * 100 \quad (14)$$

3.4. WCE Image Classification

The ELM approach was utilised in the last phase of the WCE image classification process. ELM mapped input instances to their resultant labels with single feedforward hidden layer [24]. The input-weighted linking input and hidden nodes can be created arbitrarily and never upgraded. Fig. 2 showcases the infrastructure of ELM. The resultant weighted linking output and hidden nodes are commonly learned by resolving a linear least-squares optimizer problem. Assume $X = [x_1; \dots; x_i; \dots; \dots x_m] \in \Re^{m \times n}$ be trained instance set and $T^{\chi} = [t_1^{\chi}; \dots; t_i^{\chi}; \dots; \times_m^{\chi}] \in \Re^{m \times d}$ be its labels with m instances, whereas $x_i \in \Re^{1 \times n}$, $t_i^{\chi} \in \Re^{1 \times d}$. Provided testing instance set, $y = [y_1; \dots; y_j; \dots; y_s] \in \Re^{s \times n}$

with s instances, the processes of ELM for predicting the desired labels, $T^y = [t_1^y; \ldots; t_j^y; \ldots; t_s^y] \in \Re^{s \times d}$, are defined as:

Step1: To provide a count of hidden layer nodes, L, input weighted, $W = [w_1, \ldots, w_1, \ldots, w_L] \in \Re^{n \times L}$ whereas $w_1 \in \Re^{n \times 1}$, and the bias, $b = [b_1, \ldots, b_1, \ldots, b_L] \in \Re^{1 \times L}$, are randomly generated.

Step2: To give an activation function, g (sigmoid activation function), conceded node matrices, H_r was computed to train instances as:

$$H_r = \begin{bmatrix} h(x_1; w_1, b_1), & \cdots & h(x_1; w_l, b_l) & \ldots & h(x_1; w_L, b_L) \\ \vdots & \ldots & \vdots & \ldots & \vdots \\ h(x_m; w_1, b_1), & \ldots & h(x_m; w_l, b_l) & \cdots & h(x_m; w_L, b_L) \end{bmatrix} \in \Re^{m \times L} \quad (15)$$

$$where\ h(x_i; w_l, b_l) = g(x_i w_l + b_l$$

Step3: If H_r is non-singular, the resultant weighted matrix, B, was computed as $B = H_r^{\dagger} T^{\chi}$, whereas $H_r^{\dagger} = (H_r^T H_r)^{-1} H_r^T$ refers to the Moore-Penrose generalizing inverse of H_r.

Step4: The hidden node matrix, H_e was computed to test instances as:

$$H_e = \begin{bmatrix} h(y_1; w_1, b_1), & \cdots & h(y_1; w_l, b_l) & \ldots & h(y_1; w_L, b_L) \\ \vdots & \ldots & \vdots & \ldots & \vdots \\ h(y_m; w_1, b_1), & \ldots & h(y_m; w_l, b_l) & \cdots & h(y_m; w_L, b_L) \end{bmatrix} \in \Re^{s \times L}, \quad (16)$$

$$where\ h(y_j; w_1, b_1) = g(y_j w_l + b_l)$$

Step5: The desired matrix, T^y was computed as $T^y = H_e B$.

During this training procedure, ELM only computes the resultant weighted matrix, B, linking output and hidden nodes with a minimum-squares approach. It proposes the benefits of rapid training speediness and better global searching capability. Additionally, the generalized efficiency of ELM was verified by Bartlett's model.

4. Results Analysis

The experimental outcomes of the WCEIC-RSADL method can be investigated on the database, encompassing 300 WCE images, as shown in Table 1. Fig. 3 depicts the trial imageries.

Table 1. Details of dataset

Class Name	No. of Images
Normal	150
Infected	150
Total Images	**300**

The confusion matrix of the WCEIC-RSADL technique is given in Fig. 4. The outcomes identify that the WCEIC-RSADL approach has correctly perceived the general and infected trials. For example, with 90% of TRP, the WCEIC-RSADL approach has detected 130 normal instances and 135 infected instances. In addition, with 10% of TSP, the WCEIC-RSADL system has detected 16 normal instances and 13 infected instances. Concurrently, with 80% of TSP, the WCEIC-RSADL method has detected 123 normal instances and 114 infected instances. Similarly, with 20% of TSP, the WCEIC-RSADL technique has detected 27 normal instances and 32 infected instances.

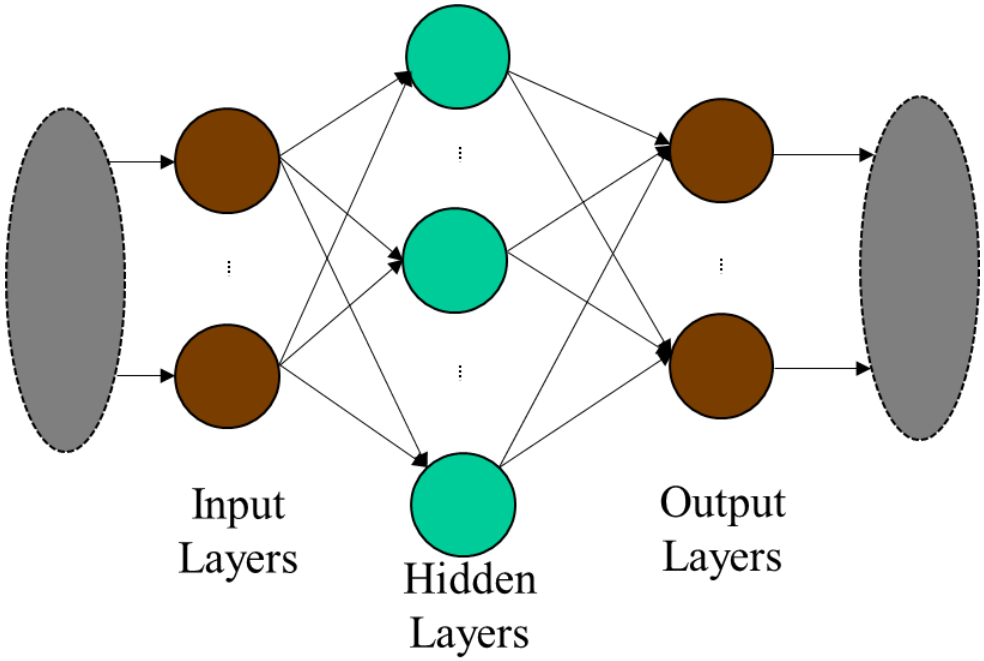

Fig. 2 Structure of ELM

Fig. 3 Sample images

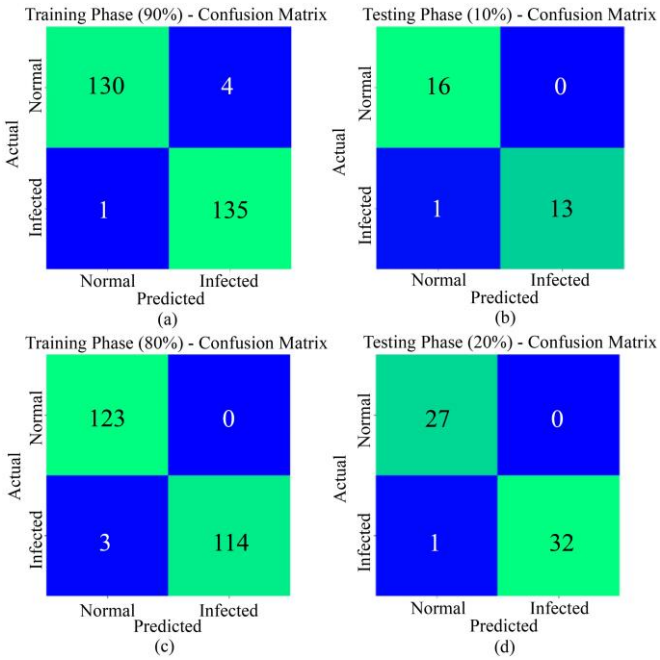

Fig. 4 Confusion matrix of WCEIC-RSADL model (a-b) TRP/TSP of 90:10 and (c-d) TRP/TSP of 80:20

In Table 2, the outputs of the sWCEIC-RSADL model can be studied under 90:10 of TRP/TSP. Fig.5 depicts the categorization outcomes of the WCEIC-RSADL technique under 90% of TRP. The outcomes show that the WCEIC-RSADL approach has precisely classified the normal and infected samples. In addition, it is noticed that the WCEIC-RSADL technique obtains average $accu_{bal}$ of 98.14%, $prec_n$ of 98.18%, $reca_l$ of 98.14%, F_{score} of 98.15%, and G_{mean} of 98.13%.

Fig. 6 depicts the categorization outcomes of the WCEIC-RSADL approach under 10% of TSP. The results show that the WCEIC-RSADL method has accurately classified the normal and infected samples. In addition, it is noticed that the WCEIC-RSADL approach obtains average $accu_{bal}$ of 96.43%, $prec_n$ of 97.06%, $reca_l$ of 96.43%, F_{score} of 96.63%, and G_{mean} of 96.36%.

In Table 3, the results of the WCEIC-RSADL technique can be studied under 80:20 of TRP/TSP. Fig. 7 denotes the categorization outcomes of the WCEIC-RSADL approach under 80% of TRP. The outputs show that the WCEIC-RSADL model has accurately classified the normal and infected samples. Also, it is noted that the WCEIC-RSADL technique obtains average $accu_{bal}$ of 98.72%, $prec_n$ of 98.81%, $reca_l$ of 98.72%, F_{score} of 98.75%, and G_{mean} of 98.71%.

Fig. 8 represents the classification outcomes of the WCEIC-RSADL system under 20% of TSP. The outputs show that the WCEIC-RSADL approach has classified the normal and infected samples precisely. Additionally, it is noted that the WCEIC-RSADL technique obtains average $accu_{bal}$ of 98.48%, $prec_n$ of 98.21%, $reca_l$ of 98.48%, F_{score} of 98.32%, and G_{mean} of 98.47%.

Table 2. Classifier outcome of WCEIC-RSADL method on TRP/TSP of 90:10

Class	$Accu_{bal}$	$Prec_n$	$Reca_l$	F_{score}	G-Mean
Training Phase (90%)					
Normal	97.01	99.24	97.01	98.11	98.13
Infected	99.26	97.12	99.26	98.18	98.13
Average	**98.14**	**98.18**	**98.14**	**98.15**	**98.13**
Testing Phase (10%)					
Normal	100.00	94.12	100.00	96.97	96.36
Infected	92.86	100.00	92.86	96.30	96.36
Average	**96.43**	**97.06**	**96.43**	**96.63**	**96.36**

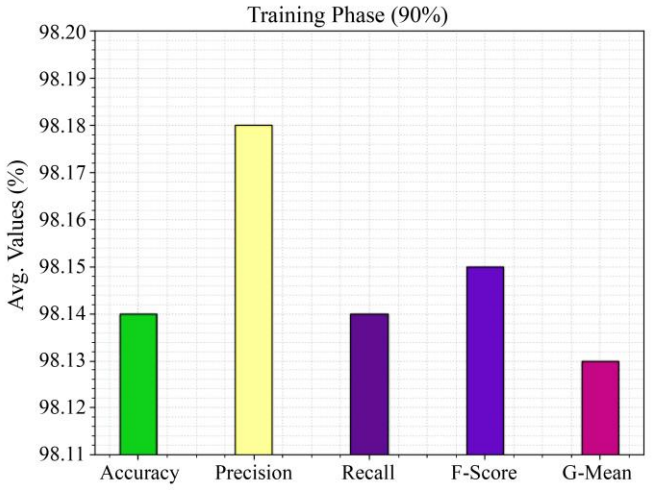

Fig. 5 Average outcome of the WCEIC-RSADL method on 90% of TRP

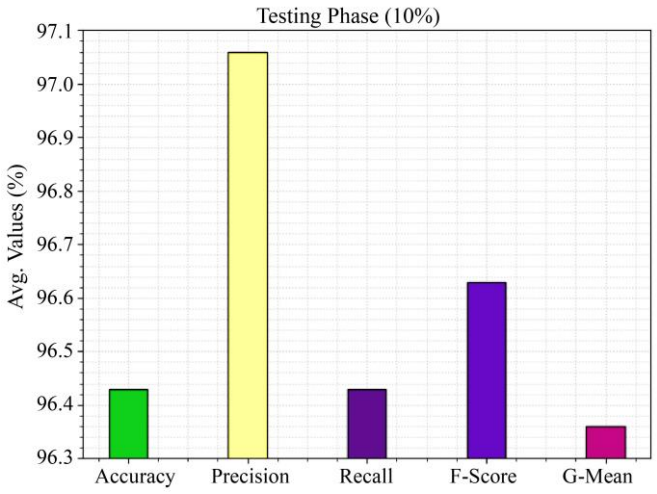

Fig. 6 Average outcome of WCEIC-RSADL approach on 10% of TSP

Table 3. Classifier outcome of WCEIC-RSADL method on TRP/TSP of 80:20

Class	$Accu_{bal}$	$Prec_n$	$Reca_l$	F_{score}	G-Mean
Training Phase (80%)					
Normal	100.00	97.62	100.00	98.80	98.71
Infected	97.44	100.00	97.44	98.70	98.71
Average	**98.72**	**98.81**	**98.72**	**98.75**	**98.71**
Testing Phase (20%)					
Normal	100.00	96.43	100.00	98.18	98.47
Infected	96.97	100.00	96.97	98.46	98.47
Average	**98.48**	**98.21**	**98.48**	**98.32**	**98.47**

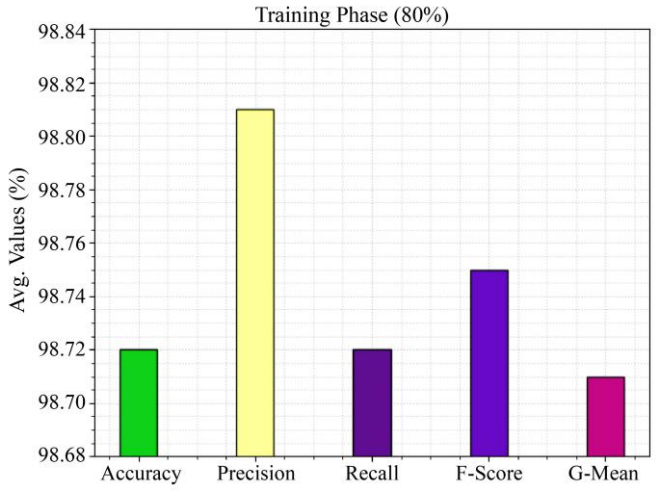

Fig. 7 Average outcome of WCEIC-RSADL approach on 80% of TRP

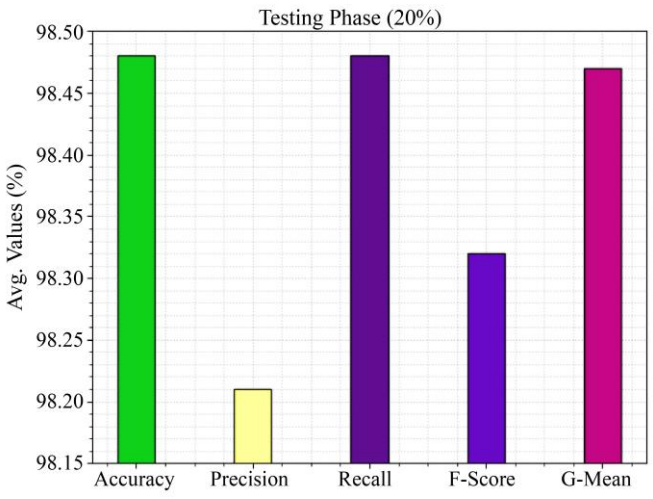

Fig. 8 Average outcome of the WCEIC-RSADL method on 20% of TSP

Fig. 9 TACY and VACY outcome of the WCEIC-RSADL method

Fig. 10 TLOS and VLOS outcome of the WCEIC-RSADL method

The TACY and VACY of the WCEIC-RSADL method are inspected on WCE achievement in Fig. 9. The outputs exhibited that the WCEIC-RSADL algorithm has enhanced achievement with improved TACY and VACY values. Notably, the WCEIC-RSADL approach has maximum TACY results.

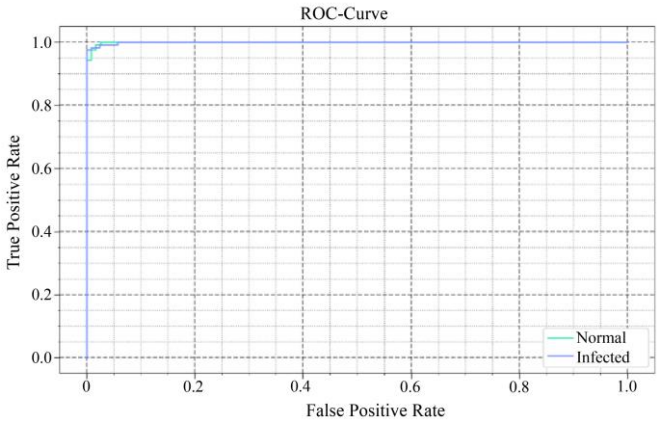

Fig. 11 Precision-recall outcome of the WCEIC-RSADL method

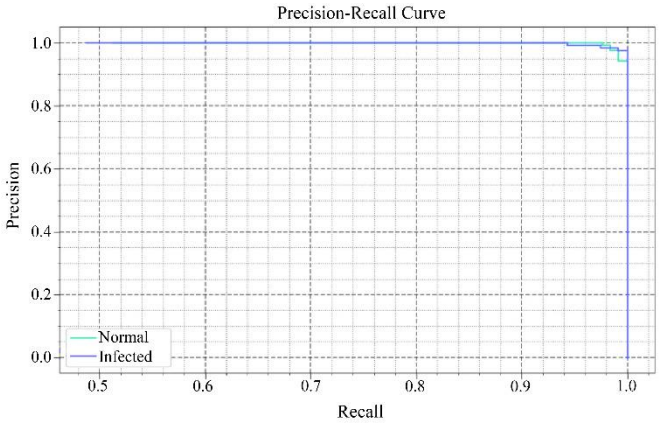

Fig. 12 ROC outcome of WCEIC-RSADL approach

The TLOS and VLOS of the WCEIC-RSADL method are inspected on WCE achievement in Fig. 10. The outputs inferred that the WCEIC-RSADL algorithm had displayed superior accomplishment with minimal TLOS and VLOS values. Especially the WCEIC-RSADL approach has the least VLOS results.

A clear precision-recall inspection of the WCEIC-RSADL approach under the trial dataset is represented in Fig. 11. The Fig. indicated that the WCEIC-RSADL approach has improved precision-recall values under each category labelling.

A short ROC study of the WCEIC-RSADL algorithm under the trial dataset is shown in Fig. 12. The outputs selected by the WCEIC-RSADL approach have revealed their capability in categorizing discrete categories.

Table 4 highlights the overall comparison study of the WCEIC-RSADL technique in terms of different measures.

Table 4. Comparative analysis of the WCEIC-RSADL algorithm with other methods

Methods	$Accu_{bal}$	$Prec_n$	$Reca_l$	F_{score}
WCEIC-RSADL	98.72	98.81	98.72	98.75
RF	96.51	97.34	97.10	97.23
ETC	93.36	93.72	93.46	92.80
LR	87.46	90.50	88.49	88.36
SVM	89.31	91.08	88.78	88.77
DTC	90.60	92.57	91.62	91.06

In Fig. 13, a relative results investigation of the WCEIC-RSADL technique can be assessed in terms of $accu_y$ and $F1_{score}$. The investigational values indicate that the WCEIC-RSADL approach outcomes in an enhanced achievement over other approaches. For instance, based on $accu_y$, the WCEIC-RSADL technique gains increasing $accu_y$ of 98.72%, whereas the SVM, LR, RF, ETC, and DTC approaches obtain reducing $accu_y$ percentage of 96.51, 93.36, 87.46, 89.31, and 90.60 subsequently.

Meanwhile, depending on $F1_{score}$, the WCEIC-RSADL technique gains increasing $F1_{score}$ of 98.75%, whereas the RF, ETC, LR, SVM, and DTC approaches obtain reducing $F1_{score}$ of 97.23%, 92.80%, 88.36%, 88.77% and 91.06% appropriately.

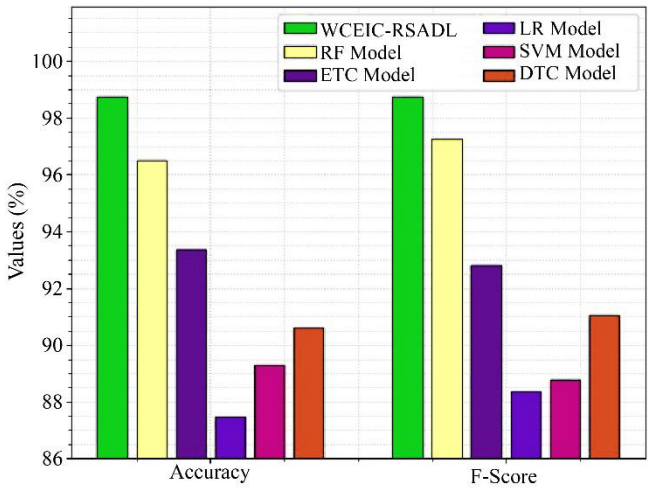

Fig. 13 $Accu_y$ and $F1_{score}$ analysis of the WCEIC-RSADL algorithm with other approaches

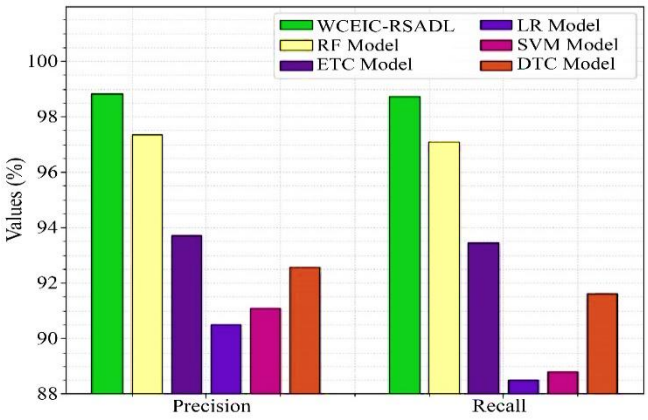

Fig. 14 $Prec_n$ and $Reca_l$ analysis of the WCEIC-RSADL algorithm with other approaches

In Fig. 14, a comparative results analysis of the WCEIC-RSADL technique can be assessed in terms of $prec_n$ and $reca_l$. The investigational values indicate that the WCEIC-RSADL model's outcomes precipitated achievement over other models. For instance, based on $prec_n$, the WCEIC-RSADL technique gains increasing $prec_n$ of 98.81%, whereas the RF, ETC, LR, SVM, and DTC approaches obtain reducing $prec_n$ of 97.34%, 93.72%, 90.50%, 91.08% and 92.57% respectively.

In the meantime, based on $reca_l$, the WCEIC-RSADL approach gains increasing $reca_l$ of 98.72%, whereas the RF, ETC, LR, SVM, and DTC approaches obtain reducing $reca_l$ of 97.10%, 93.46%, 88.49%, 88.78% and 91.62% correspondingly. Such outcomes demonstrated the improved outcomes of the WCEIC-RSADL technique.

5. Conclusion

In this article, we have established a novel WCEIC-RSADL approach for WCE image categorization. The introduced WCEIC-RSADL method mainly concentrated on categorising the WCE imageries using DL and hyperparameter tuning techniques. Primarily, the presented WCEIC-RSADL technique involves the BF technique employed for the noise elimination process. Moreover, the presented WCEIC-RSADL technique derived the Inception v2 model for feature extraction purposes with RSA-based hyperparameter tuning purposes. Furthermore, the ELM model is used for WCE image classification. In order to show the improved accomplishment of the WCEIC-RSADL approach, a series of duplications was achieved on the WCE image dataset. The simulation values highlighted that the WCEIC-RSADL method reaches promising performance over other models. In the future, the WCEIC-RSADL method's performance can be enhanced by hybrid metaheuristics.

References

[1] Deepak Bajhaiya, and Sujatha Narayanan Unni, "Deep Learning-enabled Classification of Gastric Ulcers from Wireless-capsule Endoscopic Images," *Medical Imaging 2022: Digital and Computational Pathology*, vol. 12039, 2022. [CrossRef] [Google Scholar] [Publisher link]

[2] Prabhananthakumar Muruganantham, and Senthil Murugan Balakrishnan, "A Survey on Deep Learning Models for Wireless Capsule Endoscopy Image Analysis," *International Journal of Cognitive Computing in Engineering*, vol. 2, pp. 83-92, 2021. [CrossRef] [Google Scholar] [Publisher link]

[3] Muhammad Attique Khan et al., "Computer-aided Gastrointestinal Diseases Analysis from Wireless Capsule Endoscopy: A Framework of Best Features Selection," *IEEE Access*, vol. 8, pp. 132850-132859, 2020. [CrossRef] [Google Scholar] [Publisher link]

[4] Vrushali Raut, and Reena Gunjan, "Transfer Learning Based Video Summarization in Wireless Capsule Endoscopy," *International Journal of Information Technology*, vol. 14, pp. 2183-2190, 2022. [CrossRef] [Google Scholar] [Publisher link]

[5] Tang-Kai Yin et al., "Endoscopy Artefact Detection by Deep Transfer Learning of Baseline Models," *Journal of Digital Imaging*, vol. 35, pp. 1101-1110, 2022. [CrossRef] [Google Scholar] [Publisher link]

[6] Ramya Ravibarathi, and Tamilarasu Viswanathan, "Assimilation of Gesture using 9 Axis Acclerometer Sensor," *SSRG International Journal of Electrical and Electronics Engineering*, vol. 5, no. 2, pp. 1-4, 2018. [CrossRef] [Google Scholar] [Publisher link]

[7] S. Jain, A. Seal, and A. Ojha, *Deep Learning Models for Anomaly Detection in Wireless Capsule Endoscopy Video Frames: The Transfer Learning Approach*, Smart Computing, CRC Press, 2021. [Google Scholar] [Publisher link]

[8] Dallel Bouyaya, Said Benierbah, and Mohammed Khamadja, "An Intelligent Compression System for Wireless Capsule Endoscopy Images," *Biomedical Signal Processing and Control*, vol. 70, p.102929, 2021. [CrossRef] [Google Scholar] [Publisher link]

[9] Shaik Abdul Khalandar Basha et al., "A Novel Approach to Analysis Consequence of Climate changes on Erythemato-squamous Diseases using Machine Learning Algorithms," *International Journal of Engineering Trends and Technology*, vol. 70, no. 11, pp. 10-18, 2022. [CrossRef] [Publisher link]

[10] Swati Rane et al., "Image Denoising using Adaptive Patch Clustering with Suboptimal Wiener Filter in PCA Domain," *International Journal of Engineering Trends and Technology*, vol. 70, no. 11, pp. 19-27, 2022. [CrossRef] [Google Scholar] [Publisher link]

[11] M.R. Banwaskar, and A.M. Rajurkar, "An Efficient Flower Classification System using Feature Fusion," *International Journal of Engineering Trends and Technology*, vol. 70, no. 11, pp. 70-80, 2022. [CrossRef] [Google Scholar] [Publisher link]

[12] Meryem Souaidi, and Mohamed El Ansari, "Multi-scale Hybrid Network for Polyp Detection in Wireless Capsule Endoscopy and Colonoscopy Images," *Diagnostics*, vol. 12, no. 8, p. 2030, 2022. [CrossRef] [Google Scholar] [Publisher link]

[13] M.N. Rajesh, and B.S. Chandrasekar, "Deep Learning-Based Semantic Segmentation Models for Prostate Gland Segmentation," *SSRG International Journal of Electrical and Electronics Engineering*, vol. 10, no. 2, pp. 157-171, 2023. [CrossRef] [Publisher link]

[14] Prabhananthakumar Muruganantham, and Senthil Murugan Balakrishnan, "Attention Aware Deep Learning Model for Wireless Capsule Endoscopy Lesion Classification and Localization," *Journal of Medical and Biological Engineering*, vol. 42, pp.157-168, 2022. [CrossRef] [Google Scholar] [Publisher link]

[15] Samir Jain, Ayan Seal, and Aparajita Ojha, "A Hybrid Convolutional Neural Network with Meta Feature Learning for Abnormality Detection in Wireless Capsule Endoscopy Images," *arXiv preprint arXiv:2207.09769*, 2022. [CrossRef] [Google Scholar] [Publisher link]

[16] Syeda Sara Samreen, and Hakeem Aejaz Aslam, "Hyperspectral Image Classification using Deep Learning Techniques: A Review," *SSRG International Journal of Electronics and Communication Engineering*, vol. 9, no. 6, pp. 1-4, 2022. [CrossRef] [Publisher link]

[17] Esmaeil S. Nadimi et al., "Application of Deep Learning for Autonomous Detection and Localization of Colorectal Polyps in Wireless Colon Capsule Endoscopy," *Computers & Electrical Engineering*, vol. 81, p. 106531, 2020. [CrossRef] [Google Scholar] [Publisher link]

[18] Abbas Biniaz, Reza Aghaeizadeh Zoroofi, and Masoud Reza Sohrabi, "Automatic Reduction of Wireless Capsule Endoscopy Reviewing Time Based on Factorization Analysis," *Biomedical Signal Processing and Control*, vol. 59, p. 101897, 2020. [CrossRef] [Google Scholar] [Publisher link]

[19] V. Banupriya, and S. Anusuya, "Improving Classification of Retinal Fundus Image Using Flow Dynamics Optimized Deep Learning Methods," *SSRG International Journal of Electrical and Electronics Engineering*, vol. 9, no. 12, pp. 39-48, 2022. [CrossRef] [Publisher link]

[20] Meryem Souaidi, and Mohamed El Ansari, "Automated Detection of Wireless Capsule Endoscopy Polyp Abnormalities with Deep Transfer Learning and Support Vector Machines," *International Conference on Advanced Intelligent Systems for Sustainable Development*, pp. 870-880, 2020. [CrossRef] [Google Scholar] [Publisher link]

[21] Keshetti Sreekala et al., "Capsule Network-based Deep Transfer Learning Model for Face Recognition," *Wireless Communications and Mobile Computing*, 2022. [CrossRef] [Google Scholar] [Publisher link]

[22] Syntia Widyayunigtias Putri Listio, "Performance of Deep Learning Inception Model and MobileNet Model on Gender Prediction through Eye Image," *Synchronous: Journal of Informatics Engineering and Research*, vol. 7, no. 4, 2022. [CrossRef] [Google Scholar] [Publisher link]

[23] Muhammad Kamran Khan et al., "Improved Reptile Search Optimization Algorithm: Application on Regression and Classification Problems," *Applied Sciences*, vol. 13, no. 2, p. 945, 2023. [CrossRef] [Google Scholar] [Publisher link]

[24] Lei Wang, Hongrui Cao, and Yang Fu, "A Bearing Prognosis Framework Based on Deep Wavelet Extreme learning Machine and Particle Filtering," *Applied Soft Computing*, vol. 131, p. 109763, 2022. [CrossRef] [Google Scholar] [Publisher link]